# CHAPTER 2

# NUCLEAR QUADRUPOLE RESONANCE SPECTROSCOPY

Bryan H. Suits
Physics Department, Michigan Technological University, Houghton, MI, USA

## 2.1 INTRODUCTION

Nuclear quadrupole resonance (NQR) uses radio-frequency (RF) magnetic fields to induce and detect transitions between sublevels of a nuclear ground state, a description that also applies to nuclear magnetic resonance (NMR). NMR refers to the situation where the sublevel energy splitting is predominantly due to a nuclear interaction with an applied static magnetic field, while NQR refers to the case where the predominant splitting is due to an interaction with electric field gradients within the material. So-called "pure NQR" refers to the common case when there is no static magnetic field at all.

The beginning of NQR in solids dates back to the beginnings of NMR in the late 1940s and early 1950s [1]. The first NQR measurements reported for a solid were by Dehmelt and Kruger using signals from $^{35}$Cl in trans-dichloroethylene [2]. An excellent early summary of NQR theory and technique can be found in the 1958 book by Das and Hahn [3]. Several more recent summaries can be found listed at the end of this chapter. Due to practical limitations, discussed below, NQR has not grown to be nearly as common as NMR, and is usually considered a tool for the specialist.

As is the case for NMR spectroscopy, the primary goal for NQR spectroscopy is to determine nuclear transition frequencies (i.e., energies) and/or relaxation times and then to relate those to a property of a material being studied. That property may simply be the sample temperature, for use as an NQR thermometer [4, 5], or even whether or not a sample is present when NQR is used for materials detection [6]. On the other hand, NQR is also used to obtain detailed information on crystal symmetries and bonding, on changes in lattice constants with pressure, about phase transitions in solids, and other properties of materials of interest to solid state physicists and chemists.

As will be seen in more detail below, in order to use NQR spectroscopy one must have available an isotope with a nuclear spin $I > \frac{1}{2}$, which has a reasonably high isotopic abundance, and which is at a site in a solid that has symmetry lower than tetragonal. The most common NMR isotopes, $^1H$, $^{13}C$, and $^{15}N$ cannot be used since they have a nuclear spin $\frac{1}{2}$. Of course, $^{12}C$ and $^{16}O$ cannot be used either as they have nuclear spin 0. Table 2.1 shows a selection of potential nuclei including those most commonly used for NQR, as well as a few others of possible interest.

## 2.2  BASIC THEORY

### 2.2.1 The Nuclear Electric Quadrupole Interaction

Since a nuclear wavefunction has a definite state of parity, a multipole expansion of the fields due to the nucleus yields electric $2^n$-poles, where $n$ is even (monopole, quadrupole, etc.) and magnetic $2^n$-poles, where $n$ is odd (dipoles, octupoles, etc.). In general these multipole moments become weaker very rapidly with increasing $n$. In a molecule or in a solid, the nucleus will be at an equilibrium position where the electric field is zero, and so in the absence of a magnetic field the first non-zero interaction is with the electric quadrupole moment of the nucleus. Higher moments, if they exist, are generally much too weak to affect NQR measurements [7–9].

A non-zero electric quadrupole moment arises for nuclei that are classically described as prolate ("stretched") or oblate ("squashed") spheroids. The nuclear charge distribution has axial symmetry and the axis of symmetry coincides with the direction of the nuclear angular momentum and the nuclear magnetic dipole moment. In general, an electric quadrupole moment is described by a $3 \times 3$ symmetric, traceless tensor $\mathbf{Q}$. For a nucleus such a tensor can be determined using a single value that describes how prolate or oblate the nucleus is, plus a description of the orientation of the nucleus. Since the charge distribution for a nucleus with spin 0 or $\frac{1}{2}$ is spherical, such nuclei will have no electric quadrupole moment.

If the charge distribution within the nucleus is known, the amount by which the sphere is prolate or oblate is determined by the (scalar) nuclear quadrupole moment $Q$, which can be calculated using

$$eQ = \int \rho \, (3z^2 - r^2) \, d\tau \qquad (2.1)$$

where the $z$-axis is along the direction of axial symmetry, $e$ is the magnitude of the charge on an electron, and $\rho$ is the nuclear charge density as a function of position. While such computations may be done by a nuclear physicist to check a new model for the nucleus, the NQR spectroscopist uses values determined experimentally. Values of $Q$ are conveniently expressed in units of $10^{-24}$ cm$^2$ = 1 barn.

**Table 2.1** Selected quadrupolar nuclei.

| Nucleus | Natural Isotopic Abundance % | Spin $I$ | $\gamma/2\pi$ (kHz/G) | $Q$ $(10^{-24}\,\text{cm}^2)$ |
|---|---|---|---|---|
| $^{2}$H | 0.015 | 1 | 0.654 | +0.00286 |
| $^{6}$Li | 7.4 | 1 | 0.626 | −0.0008 |
| $^{7}$Li | 92.6 | 3/2 | 1.655 | −0.040 |
| $^{10}$B | 19.6 | 3 | 0.458 | +0.085 |
| $^{11}$B | 80.4 | 3/2 | 1.366 | +0.041 |
| $^{14}$N | 99.6 | 1 | 0.308 | +0.019 |
| $^{17}$O | 0.048 | 5/2 | −0.577 | −0.26 |
| $^{23}$Na | 100 | 3/2 | 1.126 | +0.10 |
| $^{27}$Al | 100 | 5/2 | 1.109 | +0.14 |
| $^{35}$Cl | 75.5 | 3/2 | 0.417 | −0.082 |
| $^{37}$Cl | 24.5 | 3/2 | 0.347 | −0.064 |
| $^{50}$V | 0.25 | 6 | 0.425 | +0.21 |
| $^{51}$V | 99.8 | 7/2 | 1.119 | −0.05 |
| $^{55}$Mn | 100 | 5/2 | 1.050 | +0.33 |
| $^{59}$Co | 100 | 7/2 | 1.005 | +0.40 |
| $^{63}$Cu | 69.1 | 3/2 | 1.128 | −0.21 |
| $^{65}$Cu | 30.9 | 3/2 | 1.209 | −0.195 |
| $^{69}$Ga | 60.4 | 3/2 | 1.022 | +0.17 |
| $^{71}$Ga | 39.6 | 3/2 | 1.298 | +0.10 |
| $^{75}$As | 100 | 3/2 | 0.729 | +0.31 |
| $^{79}$Br | 50.5 | 3/2 | 1.067 | +0.33 |
| $^{81}$Br | 49.5 | 3/2 | 1.150 | +0.28 |
| $^{85}$Rb | 72 | 5/2 | 0.411 | +0.23 |
| $^{87}$Rb | 28 | 3/2 | 1.393 | +0.13 |
| $^{93}$Nb | 100 | 9/2 | 1.041 | −0.32 |
| $^{113}$In | 4.3 | 9/2 | 0.931 | +0.8 |
| $^{115}$In | 95.7 | 9/2 | 0.933 | +0.8 |
| $^{121}$Sb | 57.3 | 5/2 | 1.019 | −0.4 |
| $^{123}$Sb | 42.7 | 7/2 | 0.552 | −0.5 |
| $^{127}$I | 100 | 5/2 | 0.852 | −0.7 |
| $^{138}$La | 0.1 | 5 | 0.564 | +0.4 |
| $^{139}$La | 99.9 | 7/2 | 0.606 | +0.2 |
| $^{181}$Ta | 99.99 | 7/2 | 0.510 | +3.3 |
| $^{197}$Au | 100 | 3/2 | 0.073 | +0.55 |
| $^{209}$Bi | 100 | 9/2 | 0.684 | −0.4 |
| $^{235}$U | 0.72 | 7/2 | −0.076 | +5 |

While the electric field at the nucleus is zero, the electric field gradients (spatial derivatives of that field) may not be. Figure 2.1 is a schematic showing two orientations of a prolate nucleus ($Q > 0$) at a point where the electric field is zero in the vicinity of four fixed point charges. The configuration shown on the left will have a lower energy than that shown on the right since the positive charge of the nucleus is, on the whole, closer to the negative charges. When quantum mechanics is applied, this orientation dependence gives rise to a small splitting of the nuclear ground state.

a)

b)

non-spherical
nucleus
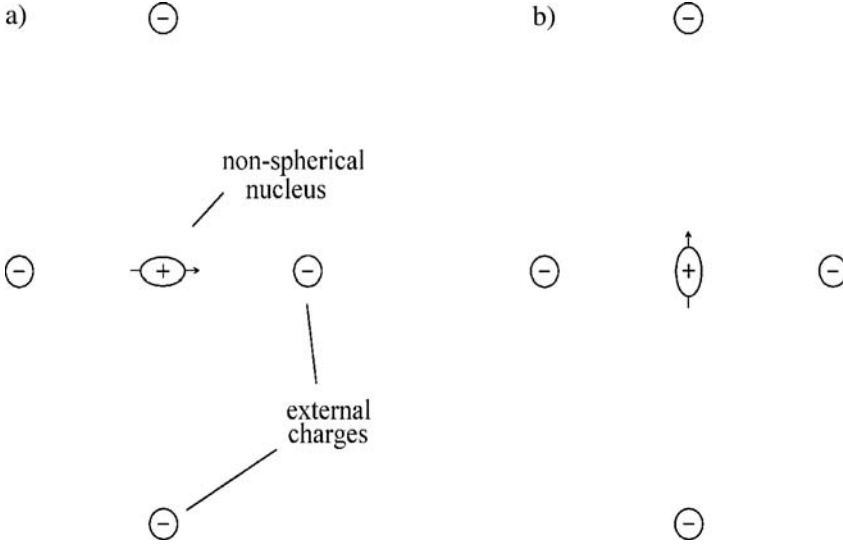
external
charges

**Figure 2.1** Two configurations of a non-spherical nucleus near charges external to the nucleus. The configuration at (a) has a lower energy than that shown at (b).

The electric field gradient at the nucleus due to charges external to the nucleus, $\nabla E$, is conveniently described using spatial derivatives of the corresponding electrostatic potential, $V$, evaluated at the nucleus. Taking the nucleus to be at the origin of the coordinate system, the desired derivatives are

$$V_{jk} = \left. \frac{\partial^2 V}{\partial r_j \partial r_k} \right|_0 \qquad (2.2)$$

where $\{r_i\} = \{x, y, z\}$. Since $V_{jk} = V_{kj}$ and, using Laplace's equation,

$$\sum_{i=x,y,z} V_{ii} = 0, \qquad (2.3)$$

the field gradient can be described by a real, symmetric, traceless $3 \times 3$ tensor. Such a tensor can always be made diagonal by choosing an appropriate set of coordinate axes known as *principal axes*. Once this is done, it is conventional to define

$$eq = V_{zz} \tag{2.4}$$

$$\eta = \frac{V_{yy} - V_{xx}}{V_{yy} + V_{xx}} = \frac{V_{xx} - V_{yy}}{V_{zz}} \tag{2.5}$$

where $\eta$ is known as the *asymmetry parameter*. It is convenient to choose the principal axes such that

$$\left| V_{xx} \right| \leq \left| V_{yy} \right| \leq \left| V_{zz} \right| \tag{2.6}$$

giving $0 \leq \eta \leq 1$. Since the principal axes are determined by the environment surrounding the nucleus, those axes are sometimes also referred to as forming a "molecular" or "crystal" coordinate system. For axial symmetry $V_{xx} = V_{yy} = -V_{zz}/2$ and $\eta = 0$.

Classically, the *interaction energy* is given by the tensor scalar product

$$E_Q = \frac{1}{6} \sum_{i,j=x,y,z} V_{ij} Q_{ij} , \tag{2.7}$$

where the two tensors must be expressed in the same coordinate system. Coordinate transformations can be accomplished using well-known relations for $3 \times 3$ symmetric tensors.

Since the nuclear state can be described by specifying the nuclear angular momentum, the entire interaction can be written, with appropriate scale factors including the scalar quadrupole moment, in terms of the angular momentum. When written using quantum mechanical operators, the Hamiltonian $\mathcal{H}_Q$ for a nucleus of spin $I$ expressed in the principal axis coordinate system is

$$\mathcal{H}_Q = \frac{e^2 q Q}{4I(2I-1)} \left[ 3I_z^2 - I^2 + \eta \left( I_x^2 - I_y^2 \right) \right]$$

where all $I$'s in the denominator are scalar values while all $I$'s in the square brackets are operators. The interested reader can find a detailed derivation of this result in Slichter's book [10]. In terms of the usual angular momentum raising and lowering operators, $I_\pm = I_x \pm i I_y$, the Hamiltonian can also be written

$$\mathcal{H}_Q = \frac{e^2 q Q}{4I(2I-1)} \left[ 3I_z^2 - I^2 + \eta \cdot \frac{I_+^2 - I_-^2}{2} \right] . \tag{2.8}$$

To represent the Hamiltonian in other coordinate systems, the appropriate angular momentum rotation operators are applied. Other forms for the operators, such as irreducible tensor operators, are also sometimes employed (see [11] for example).

One of the goals of an NQR measurement will be to determine the quadrupole coupling constant $e^2 q Q$ and the asymmetry parameter $\eta$, which contain information about the environment surrounding the nucleus.

## 2.2.2 Energy Levels and Transition Frequencies

In the case of axial symmetry, $\eta = 0$, the pure quadrupole Hamiltonian is easily diagonalized using eigenfunctions of the operator $I_z$ with quantum number $m = -I, -I + 1, \ldots, I - 1, I$. The resulting $2I + 1$ energy levels are given by

$$E_m = \frac{e^2 qQ}{4I(2I-1)} \left(3m^2 - I(I+1)\right).$$  \hfill (2.9)

In this case $m$ is a good quantum number and the usual magnetic dipole transition rules apply, $\Delta m = 0, \pm 1$. Defining

$$\nu_Q = \frac{3e^2 qQ}{4I(2I-1)h} \, ,$$  \hfill (2.10)

where $h$ is Plank's constant, the allowed transition frequencies are given by

$$\nu_{m,m\pm 1} = \nu_Q \left|(2m \pm 1)\right|; \ |m|, |m \pm 1| \le I.$$  \hfill (2.11)

For the more general case of arbitrary $\eta$, closed form solutions are known only for $I = 1$ and $I = 3/2$. Due to the symmetry of the Hamiltonian, all the energy levels are doubly degenerate for half-integer spin nuclei. For integer spin nuclei, of which there are very few in practice, there are an odd number of levels and the degeneracy is broken. Furthermore, since the eigenfunctions of $I_z$ are not, in general, energy eigenfunctions, additional transitions are often allowed.

### 2.2.2.1 Integer Spins

There are only four known stable nuclei with integer spin: $^2$H, $^6$Li, and $^{14}$N, all with $I = 1$, and $^{10}$B with $I = 3$. In addition there are some very long-lived radioactive isotopes, such as $^{50}$V, with $I = 6$ and $^{138}$La with $I = 5$. Most of the NQR work done using integer spin nuclei is for ~100% naturally abundant $^{14}$N. Deuterium ($^2$H) and $^6$Li have very small electric quadrupole moments, making direct observation with NQR difficult. There has been some work using $^{10}$B but due to its lower natural abundance compared to $^{11}$B ($I = 3/2$) the latter is preferred. The long-lived radioactive isotopes also have a very low natural abundance making them quite difficult to use.

For spin 1, the three energy levels are

$$E_0 = -\frac{2}{3}h\nu_Q, \quad E_\pm = \frac{(1 \pm \eta)}{3}h\nu_Q,$$  \hfill (2.12)

and all three possible transition frequencies

$$\nu_0 = \frac{2}{3}\eta\nu_Q \, , \quad \nu_\pm = \left(1 \pm \frac{\eta}{3}\right)\nu_Q,$$  \hfill (2.13)

are allowed.

For spin 3 an exact solution is not known. Butler and Brown [12] provide a graphical representation showing 18 allowed transitions, arising from the 7 energy levels, as a function of $\eta$. Five of those 18 are forbidden when $\eta = 0$ and are somewhat inappropriately referred to as "multiple quantum transitions." They are allowed single quantum transitions, though some are quite weak, and can be useful to help unravel the wonderfully complicated $^{10}$B NQR spectra [13].

### 2.2.2.2 Spin 3/2

Much of the NQR work in the literature is for spin 3/2 nuclei, which have two doubly degenerate energy levels,

$$E_{\pm 3/2} = h\nu_Q \left(1 + \frac{\eta^2}{3}\right)^{1/2}, \quad E_{\pm 1/2} = -h\nu_Q \left(1 + \frac{\eta^2}{3}\right)^{1/2} \qquad (2.14)$$

and hence only one (non-zero frequency) transition,

$$\nu = 2\nu_Q \left(1 + \frac{\eta^2}{3}\right)^{1/2}. \qquad (2.15)$$

The fact that there is only one frequency means that one cannot determine the two values $\nu_Q$ and $\eta$ with a simple pure NQR measurement. The application of a small magnetic field, discussed below, is often used to separately determine the two values. For many compounds studied using spin 3/2 NQR, $\eta$ has not been separately determined. Often such data are interpreted using the assumption $\eta = 0$, which can yield a maximum error of about 16% in the determination of $\nu_Q$.

### 2.2.2.3 Other Half-Integer Spins

Exact solutions are not known for $I > 3/2$. Tabulated results can be used [14], or it is now quite easy to diagonalize the Hamiltonian numerically. Expansions valid for smaller values of $\eta$ are also available [15, 16]. Results of numerical computations for half-integer spins 5/2, 7/2, and 9/2 are shown in Figure 2.2. As is customary, the levels are labeled according to the largest component of the wavefunction, though $m$ is only a good quantum number when $\eta = 0$. In addition, when $\eta \neq 0$ virtually all possible transitions are allowed though many are extremely weak. This is similar to what occurs for $^{10}$B, mentioned above. The dotted lines in Figure 2.2 indicate some of these weaker transitions, which are not allowed at all when $\eta = 0$ but which may be usable for large $\eta$. Those weaker transitions are rarely used in practice but can be helpful when disentangling spectra observed for samples with multiple sites having large $\eta$ (for example, see [17]).

When $\eta = 1$ it is possible, with some effort, to obtain exact solutions for half-integer spins up to $I = 9/2$. The resulting energy levels for these $I$ are

$$I = 5/2: \quad 0, \pm\sqrt{112/9}$$
$$I = 7/2: \quad \pm 2\left[7 \pm 4\sqrt{7/3}\right]^{1/2} \tag{2.16}$$
$$I = 9/2: \quad 0, \pm 2\left[22 \pm \sqrt{748/3}\right]^{1/2}$$

in units of $h\nu_Q$.
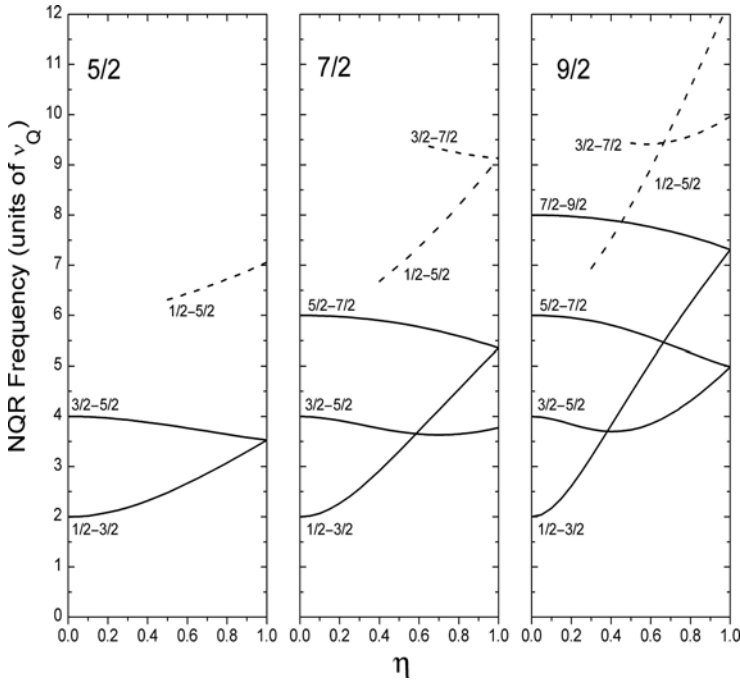


**Figure 2.2** NQR transition frequencies for spins 5/2, 7/2, and 9/2. The dashed lines are weaker transitions, which are forbidden when $\eta = 0$.

## 2.2.3 Excitation and Detection

In a typical NQR measurement transitions are induced between energy levels via the coupling between the nuclear magnetic dipole moment and a resonant time-dependent magnetic field, as is done for NMR. One could also imagine applying a time-dependent electric field gradient, however the required field strengths are much too large to be practical in the laboratory. The required time-dependent electric field gradients can be generated

indirectly by applying acoustic energy, a method important for the spectroscopic technique known as nuclear acoustic resonance (NAR) [18]. Due to practical considerations, NAR has proven to have limited utility.

To couple to the nuclear magnetic moment, the sample is placed within the RF magnetic field produced by an inductor which is carrying an alternating current (AC) of angular frequency, $\omega_r = 2\pi\nu_r$. Most commonly this is done by placing the sample within a solenoid that is part of a tuned circuit. If the AC magnetic field produced is uniform with magnitude, $B_1$, and is in the $x'$-direction in a laboratory reference frame, the *interaction Hamiltonian* is

$$\mathcal{H}_1 = \gamma B_1 I_{x'} \cos(\omega_r t + \phi)$$

where $\gamma$ is the gyromagnetic (or magnetogyric) ratio for the nucleus, $I_{x'}$ is the angular momentum operator for the component along the $x'$-direction, and $\phi$ is a phase factor.

For convenience, the energy eigenfunctions in the absence of the AC field, $\psi_n$, with energy $E_n = \hbar\omega_n$, can be expressed in terms of the eigenfunctions of $I_z$, $u_m$, where $z$ corresponds to the $z$-direction of the principal axes system. That is,

$$\psi_n = \sum_{m=-I}^{I} b_{n,m} u_m. \tag{2.17}$$

Then in turn, the total time-dependent wavefunction can be written

$$\Psi(t) = \sum_n a_n(t)\, \psi_n \exp(-i\omega_n t), \tag{2.18}$$

where the complex coefficients $a_n(t)$ are to be determined. As written, those coefficients will be time-independent when the AC magnetic field is off. Since the AC magnetic field yields a relatively weak interaction $\mathcal{H}_1$, compared to that of the static electric quadrupole field $\mathcal{H}_Q$, the coefficients $a_n$ will vary relatively slowly with time. Placing the total wavefunction into Schrödinger's time-dependent wave equation,

$$-\frac{\hbar}{i}\frac{\partial\Psi}{\partial t} = \left(\mathcal{H}_Q + \mathcal{H}_1\right)\Psi, \tag{2.19}$$

and using the orthogonality of the eigenfunctions, the coupled equations for the coefficients, $a_n(t)$, are obtained,

$$\frac{\partial a_j}{\partial t} = \frac{i\gamma B_1}{2}\sum_k a_k \left\langle \psi_j \middle| I_{x'} \middle| \psi_k \right\rangle \left\{ e^{-i\left(\omega_k - \omega_j - \omega_r\right)t + i\phi} + e^{-i\left(\omega_k - \omega_j + \omega_r\right)t - i\phi} \right\}, \tag{2.20}$$

where $\left\langle \psi_j \middle| I_{x'} \middle| \psi_k \right\rangle$ is a constant. Expressing $I_{x'}$ in the principal axes system as

$$I_{x'} = c_x I_x + c_y I_y + c_z I_z \tag{2.21}$$

where the $c_i$ are a shorthand notation for the directional cosines, then

$$\left\langle \psi_j \left| I_{x'} \right| \psi_k \right\rangle = \sum_m \left\{ m \, c_z \, b^*_{j,m} b_{k,m} \right.$$

$$+ \left( c_x - i c_y \right) \left( I(I+1) - m(m+1) \right)^{1/2} \frac{b^*_{j,m+1} b_{k,m}}{2}$$

$$\left. + \left( c_x + i c_y \right) \left( I(I+1) - m(m+1) \right)^{1/2} \frac{b^*_{j,m-1} b_{k,m}}{2} \right\}. \tag{2.22}$$

Thus far there has been no approximation.

For simplicity, assume that just two states, labeled 1 and 2, with $E_2 > E_1$, are involved. The "slowly varying" part of the solution desired occurs when the time dependence in one of the exponentials becomes small. That will occur when the frequencies in one of the exponentials nearly cancel. The other exponentials will produce rapidly oscillating terms which will tend to average to zero. Keeping only the slowly varying terms, defining $\Omega = \gamma B_1 \left\langle \psi_1 \left| I_{x'} \right| \psi_2 \right\rangle e^{i\phi}$ and $\Delta\omega = \omega_r - (\omega_2 - \omega_1)$, the two coupled equations that result are

$$\frac{\partial a_1}{\partial t} = \frac{i\Omega}{2} a_2 \, e^{-i\Delta\omega t}$$

$$\frac{\partial a_2}{\partial t} = \frac{i\Omega^*}{2} a_1 \, e^{+i\Delta\omega t} \tag{2.23}$$

which have solution

$$a_1(t) = e^{+i\Delta\omega t/2} \left[ a_1(0)\cos\left(\frac{\omega_{\text{eff}} t}{2}\right) + i \, \frac{\Omega \, a_2(0) - \Delta\omega \, a_1(0)}{\omega_{\text{eff}}} \sin\left(\frac{\omega_{\text{eff}} t}{2}\right) \right]$$

$$a_2(t) = e^{-i\Delta\omega t/2} \left[ a_2(0)\cos\left(\frac{\omega_{\text{eff}} t}{2}\right) + i \, \frac{\Omega^* a_1(0) + \Delta\omega \, a_2(0)}{\omega_{\text{eff}}} \sin\left(\frac{\omega_{\text{eff}} t}{2}\right) \right]$$

$$\tag{2.24}$$

where $a_1(0)$ and $a_2(0)$ are initial values at $t = 0$, and $\omega_{\text{eff}} = \sqrt{|\Omega|^2 + (\Delta\omega)^2}$ .

The detection of the signal is also done using a coupling to the nuclear magnetic dipole moment. Knowing the wavefunction, we can compute the expectation value of the nuclear magnetic moment, $\vec{\mu}$, at any time. The component which is along the direction $x'$ is given by

$$\left\langle \mu_{x'} \right\rangle = \gamma\hbar \sum_{j,k} a^*_j \, a_k \left\langle \psi_j \left| I_{x'} \right| \psi_k \right\rangle e^{-i(\omega_k - \omega_j)t} . \tag{2.25}$$

The total *nuclear magnetization* from $N$ such nuclei, $M_{x'}$, can be written in terms of the ensemble average

$$M_{x'} = \gamma \hbar N \sum_{j,k} \left\langle a_j^* a_k \right\rangle \left\langle \psi_j \left| I_{x'} \right| \psi_k \right\rangle e^{-i(\omega_k - \omega_j)t} \; .$$

The set of values $\left\langle a_j^* a_k \right\rangle$ are, of course, the elements of the density matrix.

A time-dependent magnetization will generate an *electromotive force* (EMF, a voltage) $V(t)$, in a nearby inductor by Faraday's law of induction. If this inductor is the same one used above for excitation, then by reciprocity,

$$V(t) \propto \frac{dM_{x'}}{dt} . \qquad (2.26)$$

A signal measured this way must arise from terms above where $j \neq k$. In thermal equilibrium $\left\langle a_j^* a_k \right\rangle$ will be zero for all $j \neq k$; after all, one cannot expect to continually extract electrical power in equilibrium. The role of the excitation is to disturb the thermal equilibrium so that a signal can be observed.

A common method to measure NQR signals is the pulse method where a relatively large AC magnetic field ($B_1 \approx 1$ to $100$ G) is applied for a short time ($\tau_p \approx 1$ to $100$ μs), after which the EMF induced in the coil is detected. The other extreme is to continuously supply a low level AC magnetic field ($B_1 < 1$ G). In that case the transitions produced are balanced against those of thermal relaxation processes and a dynamic equilibrium is obtained. Then the steady state EMF induced by the nuclei which is in phase with the current in the inductor is equivalent to an electrical resistance, and that which is out of phase a reactance. Instrumentation will be discussed in more detail in the next section.

NQR is usually performed one transition at a time and hence any of these problems can be treated using the "effective spin 1/2" formalism [19, 20]. However, it is useful to consider what happens explicitly for the two common cases of $I = 1$ and $I = 3/2$ without using that formalism.

### 2.2.3.1 Example—Spin 1

For $I = 1$, the three energy levels and the corresponding wavefunctions are illustrated in Figure 2.3. For the sake of example, assume the transition labeled $\nu_+$ is to be excited exactly on resonance ($\Delta\omega = 0$), and take $\phi = 0$. Then $\Omega = \gamma B_1 c_x$ and

$$a_+(t) = a_+(0) \cos \frac{\Omega}{2} t + i \, a_0(0) \sin \frac{\Omega}{2} t$$

$$a_0(t) = a_0(0) \cos \frac{\Omega}{2} t + i \, a_+(0) \sin \frac{\Omega}{2} t \qquad (2.27)$$

$$a_-(t) = a_-(0),$$

which is exactly what one gets if one rotates the nucleus by an angle $\Omega t/2$ about the $x$-axis. Similar expressions are obtained for the other two transitions involving the other two axes. Such rotations are often conveniently treated using exponential operators. It is interesting that for spin 1 a simultaneous excitation of two transitions can also be described as a simple rotation of the spin [21].
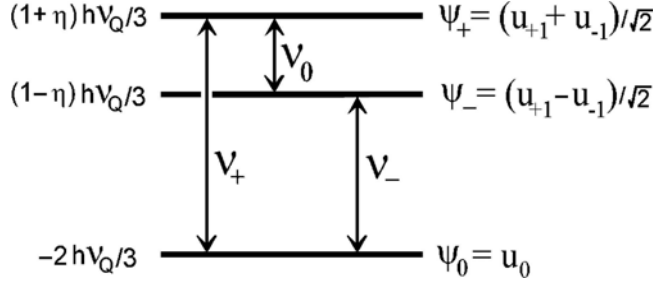


**Figure 2.3** Energy levels and transitions for spin 1.

Starting from thermal equilibrium, the EMF after a time $t$ will be

$$V(t) \propto c_x \, \omega_+ \left( \left\langle a_+^*(0) a_+(0) \right\rangle - \left\langle a_0^*(0) a_0(0) \right\rangle \right) \sin \Omega t \cos \omega_+ t , \quad (2.28)$$

which reaches a maximum at $\Omega t = \pi/2$ when the nucleus has been rotated by $\pi/4$. The term in parentheses is the population difference between the two levels determined by the Boltzmann distribution. For $^{14}$N typical energy level splittings correspond to a temperature equivalent of about 0.1 mK and hence the thermal equilibrium population difference at room temperature is only about 1 part in $10^7$.

The motion of the spin in the absence of the AC field is not easy to visualize. The simple "counter rotating" picture obtained below for $I = 3/2$ does not apply even though one can use it to some extent to form a mental picture. The classical motion of a quadrupole system is discussed by Raich and Good [22].

Note that $\Omega$ depends on sample orientation and so for powder (or polycrystalline) samples one will have a broad distribution of values. This inherently large inhomogeneity in the "effective $B_1$" (here $B_{1\text{eff}} = B_1 c_x$) occurs for NQR of powder samples, but does not occur for NMR.

## 2.2.3.2 Example—Spin 3/2

The energy levels of the spin 3/2 system are doubly degenerate. The energy levels were given above and the corresponding wavefunctions can be written

$$\psi_{\pm 3/2} = \cos\delta \; u_{\pm 3/2} \; + \; \sin\delta \; u_{\mp 1/2}$$
$$\psi_{\pm 1/2} = \cos\delta \; u_{\pm 1/2} \; - \; \sin\delta \; u_{\mp 3/2}$$

(2.29)

where $\sin\delta = \left[(\rho-1)/2\rho\right]^{1/2}$ with $\rho = \left(1+\eta^2/3\right)^{1/2}$ and the only non-zero transition frequency is $\nu = \rho\nu_Q$. In general all four transitions are allowed. However, it is always possible to create a new set of wavefunctions from linear combinations of states with the same energy. In particular,

$$\psi'_{+3/2} = A\psi_{+3/2} \; + \; B\psi_{-3/2}; \; \psi'_{-3/2} = A\psi_{-3/2} \; - \; B\psi_{+3/2} \quad (2.30)$$

and similarly for $\psi'_{\pm 1/2}$. Furthermore, a combination where only two of the four transitions are allowed can always be found. Once this has been done, the transformed spin 3/2 problem can be solved as two independent problems involving just two energy levels each [23]. The resulting classical picture for spin 3/2 NQR is that of an NMR experiment in an effective magnetic field involving the simultaneous measurement of two sets of (spin ½) nuclei, which are identical except for the sign of their gyromagnetic ratio. In the absence of the excitation one visualizes two sets of otherwise identical nuclei, precessing in opposite directions. Such a picture is a result of the degeneracy and generalizes to other half-integer spins.

The similarity between the classical picture used for NMR and that for spin 3/2 NQR leads to the use of "rotating reference frame" terminology for NQR even though it is perhaps not entirely appropriate.

## 2.2.4 The Effect of a Small Static Magnetic Field

The application of a small static magnetic field is sometimes advantageous and at other times it may simply be unavoidable. By "small" it is meant that the nuclear Zeeman interaction can be treated as a perturbation. In what follows, calculations will be carried out in the principal axes reference system. The Hamiltonian representing the Zeeman interaction can then be written

$$\mathcal{H}_z = -\gamma\hbar B_0\left(c_x I_x + c_y I_y + c_z I_z\right), \quad (2.31)$$

where the directional cosines $c_i$ may not be the same as those used previously. Any case can be treated numerically without difficulty, however it is worth taking a detailed look at spin 1 and spin 3/2 as representatives of what happens for integer and half-integer spins.

### 2.2.4.1 Spin 1

For the case of spin 1 with asymmetry parameter $\eta \neq 0$, there is no first-order shift in the energy levels. Using standard second-order perturbation theory the changes in the three transition frequencies are:

$$\Delta v_+ = \left(\frac{\gamma B_0}{2\pi v_Q}\right)^2 \left(\frac{3}{2}\frac{c_z^2}{\eta} + \frac{c_y^2}{(1-\eta/3)} + 2\frac{c_x^2}{(1+\eta/3)}\right) v_Q \qquad (2.32)$$

$$\Delta v_- = \left(\frac{\gamma B_0}{2\pi v_Q}\right)^2 \left(-\frac{3}{2}\frac{c_z^2}{\eta} + 2\frac{c_y^2}{(1-\eta/3)} + \frac{c_x^2}{(1+\eta/3)}\right) v_Q \quad (2.33)$$

$$\Delta v_0 = \left(\frac{\gamma B_0}{2\pi v_Q}\right)^2 \left(3\frac{c_z^2}{\eta} - \frac{c_y^2}{(1-\eta/3)} + \frac{c_x^2}{(1+\eta/3)}\right) v_Q, \qquad (2.34)$$

where $v_Q$ is as defined above. These are valid provided $\Delta v_0 \ll v_0$.

When $\eta = 0$, degenerate perturbation theory must be used and to lowest order one finds

$$\Delta v_\pm = \mp\frac{\gamma B_0}{2\pi} c_z \qquad (2.35)$$

$$\Delta v_0 = 2\frac{\gamma B_0}{2\pi} c_z, \qquad (2.36)$$

a result which can also be used when $\eta \neq 0$ if the first calculation yields $\Delta v_0 \gg v_0$. The intermediate case where $\Delta v_0 \approx v_0$ is more complicated and will not be treated here.

For larger magnetic fields or when a more precise result is needed, the exact but more cumbersome solutions given by Muha can be used [24].

### 2.2.4.2 Spin 3/2

NQR in the presence of a small magnetic field is a principal method used to determine the asymmetry parameter $\eta$ for spin 3/2.

The energy levels for spin 3/2, and for half-integer spins in general, will be degenerate regardless of the value of $\eta$ and hence degenerate perturbation theory must be used. The four energy levels which result for spin 3/2, in the form presented by Brooker and Creel [25], become

$$E_{\pm 3/2} = \frac{h v_Q \rho}{2} \pm \frac{h v_0}{2\rho}\left[(\rho-1+\eta)^2 c_x^2 + (\rho-1-\eta)^2 c_y^2 + (2+\rho)^2 c_z^2\right]^{1/2} \quad (2.37)$$

$$E_{\pm 1/2} = -\frac{h v_Q \rho}{2} \pm \frac{h v_0}{2\rho}\left[(\rho+1-\eta)^2 c_x^2 + (\rho+1+\eta)^2 c_y^2 + (2-\rho)^2 c_z^2\right]^{1/2} \quad (2.38)$$

where $v_0 = \gamma B_0/2\pi$. In general all the transitions between these four levels are allowed. The four transitions shown in Figure 2.4 are of most interest. The highest and lowest frequency transitions, $v_\beta$ and $v_{\beta'}$, will be somewhat "weaker" than the middle two. A computation of the transition probabilities is straightforward, though complicated enough that it will not be reproduced

here. The strength of each transition is a function of the relative orientations of the static magnetic field, the RF magnetic field, and the principal axes.

For multiple pulse measurements (described below) using a spin 3/2 nucleus in a small magnetic field one can observe an additional effect called "slow beats" [26] due to the fact that all four of these transitions are excited and they are not independent of each other.

To separately determine $\nu_Q$ and $\eta$ the transition frequencies can be measured as a function of sample orientation for single crystals or, less accurately, the spectral line shape (i.e., the frequency distribution) can be measured for powdered or polycrystalline samples [27, 28].
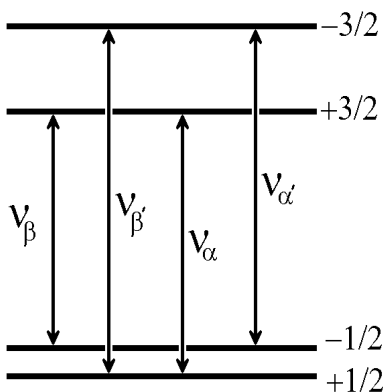


**Figure 2.4** Energy levels and transitions for spin 3/2 in a magnetic field aligned along the *z*-principle axis. The energy level splitting due to the magnetic field is greatly exaggerated.

## 2.2.5 Line Widths and Relaxation Times

In many cases the spectral line width in an NQR measurement is due to an inhomogeneous environment. That is, there is a distribution of frequencies due to small variations in the electric field gradients within the sample. The common causes for the inhomogeneity include impurities, crystal lattice defects, and even small thermal gradients within a sample. Inhomogeneous effects can be reduced through the use of carefully prepared samples and/or can be handled with pulsed methods and the spin echo techniques.

Two other important contributors to the spectral line width are dynamic effects due to motion at the atomic scale and nuclear magnetic dipole-dipole interactions These are generally referred to as "homogeneous effects" since they apply equally to all the nuclei.

As is the case for NMR, there are several different relaxation times that can be measured. The so-called *spin-spin relaxation time, $T_2$* , which may or

may not actually involve spin-spin interactions, characterizes the return of the ensemble to thermal equilibrium at some "spin temperature." The *spin-lattice relaxation time, $T_1$,* which is the inverse of the relaxation rate, characterizes the return of the ensemble of nuclei to thermal equilibrium with the surrounding crystal, usually called the "lattice." The processes which determine $T_1$ involve exchange of energy between the nuclei and their surroundings—that is nuclear transitions are induced by the (random) fluctuations of the surroundings. In contrast, the interactions that are usually most effective for $T_2$ relaxation are those where there is no (net) gain or loss of energy from the nuclear ensemble. In general several mechanisms will contribute to the relaxation.

Typically only one of several possible transitions is excited and detected for NQR and so the phrase "the return to thermal equilibrium" is usually applied in the effective spin-½ sense. That is, the thermal ensemble includes just the two nuclear energy levels used, with the remaining levels now belonging to the lattice. This can give rise to relaxation characterized by multiple exponentials. A nice derivation of the effect for Nb (I = 9/2) is given by Chen and Slichter [29].

### 2.2.5.1 Spin-Lattice Relaxation and Temperature-Dependent Frequency Shifts

The coupling between the nuclei and the surrounding crystal will be due to time-dependent magnetic and/or electric quadrupole interactions. Magnetic interactions include those due to paramagnetic impurities and, in metals, the conduction electrons. A much weaker magnetic interaction can occur via a time-dependent spin-spin interaction. For materials with two readily available isotopes (e.g., Cl, Cu, Ga, Br, Rb, Sb, etc.), whether the relaxation is dominated by magnetic or electric quadrupole interactions can usually be determined by comparing the ratio of the relaxation times to the ratios of the magnetic dipole and electric quadrupole moments, respectively, for the two isotopes.

The contribution to the relaxation by the conduction electrons in metals is due to the so-called *Korringa result*, just as in NMR [30]. Hence, this contribution is very sensitive to changes in the electron density of states at the Fermi level, such as what one expects near superconducting phase transitions [31]. Korringa relaxation is also evident in some semiconductors [32]. Paramagnetic impurities generally contribute a constant to the rate, as they do for NMR.

In many NQR measurements of non-metals, the spin-lattice relaxation time and the temperature coefficient of the NQR frequency are both a result of lattice dynamics. This can be understood using the simple model proposed by Bayer [33]. Consider an electric quadrupole Hamiltonian that has been rotated about the *y*-axis by a small angle β. The new Hamiltonian (in the old principal axis coordinates) is given by

$$\mathcal{H}_Q = \frac{\nu_Q}{6} \left[ \left( \frac{3}{2}\cos^2\beta \; - \; \frac{1}{2} \; + \; \frac{\eta}{2}\sin^2\beta \right) \; (3I_z^2 \; - \; I^2) \right.$$

$$+ (3-\eta)\sin 2\beta \; (I_z(I_+ + I_-) + (I_+ + I_-)I_z)$$

$$\left. + \frac{1}{4}\left( 3\sin^2\beta \; + \; \eta\,(1+\cos^2\beta) \right) \; (I_+^2 \; + \; I_-^2) \right] \qquad (2.39)$$

and if $\beta$ represents a small, rapid oscillation about an equilibrium at $\beta = 0$, then one can expand and take a time average to determine the average coupling. Keeping the lowest non-zero terms one gets an average of

$$\mathcal{H}_Q = \frac{\nu_Q}{6}\left[ \left( 1 - \langle\beta^2\rangle\frac{3+\eta}{2} \right) \; \left( 3I_z^2 - I^2 \right) \; + \; \frac{1}{2}\left( \eta + \langle\beta^2\rangle \; \frac{3+\eta}{2} \right) \; \left( I_+^2 + I_-^2 \right) \right]$$

and one can expect that $\langle\beta^2\rangle$ increases with temperature. The time-dependent terms, with RMS amplitude $\langle\beta^2\rangle^{1/2}$, can give rise to nuclear transitions and hence contribute to increase the relaxation rate $1/T_1$.

  The theory of the dependence of the NQR frequency on temperature has been further developed by a number of authors [34–36]. While there are exceptions, near room temperature one can expect a temperature coefficient of order 1 kHz/K for most materials. Since NQR lines are often narrower than 1 kHz, even a small temperature change can be significant, and a small temperature gradient across the sample can significantly broaden the NQR line.

### 2.2.5.2 Spin-Spin Interactions

Nuclear magnetic dipole interactions between nuclei in a solid can produce some broadening of an NQR line, as happens for NMR. In an NMR experiment, the broadening due to the spin-spin interaction can be substantially reduced using a *magic angle spinning* (MAS) measurement. Spinning the sample is not effective for NQR and can make matters worse.

  One way to estimate the size of the spin-spin interaction is to consider the size of the magnetic field due to a neighboring nucleus, typically of order 1 Gauss in solids, and then to treat the problem as in Section 2.2.4. It is easy to predict, quite correctly, that the effects for integer spin and half-integer spin will be very different. Except in a few isolated cases, the indirect dipole-dipole coupling (*e.g.*, J-coupling), one of the cornerstones of analysis for high resolution NMR spectroscopy, is not important for pure NQR work.

  The method of moments developed by van Vleck for NMR [37], adapted to the NQR case, is often used to estimate the broadening due to the spin-spin interaction. As is the case for NMR, there are separate calculations for unlike

spins and like spins. For NQR there is an additional case for spins that are otherwise alike, but for which the directions of the principal axes are different. This latter case is sometimes referred to as "semi-like." In the semi-like case the nuclear energy levels are degenerate, as is the case for like spins, however the geometry is more complicated.

One common way to compare the different situations is to compute the second moment for the somewhat artificial case of a cubic lattice of one type of nucleus. Such a comparison for several different cases is shown in Table 2.1. The characteristic decay time will be proportional to the inverse of the square root of the second moment.

**Table 2.2** Results of some second moment calculations for NQR for the case of like nuclei in a cubic lattice of edge $d$. Results are in units of $\gamma^4 \hbar^4 / d^6$.

| Spin | Condition | Second Moment | Ref. |
|------|-----------|---------------|------|
| 1 | $\eta = 0$ | 28.2 | 40 |
| 1 | $\eta \neq 0$ | 22.1 | 40 |
| 3/2 | $\eta = 0$ | 60.0 | 38 |
| 5/2 | $\eta = 0$ | 108.1 | 39 |

For spin 1 with $\eta \neq 0$ the first-order dipole coupling to unlike nuclei is zero and second-order calculations are necessary. For ^{14}N NQR when there are nearby hydrogen nuclei, the second-order coupling to the hydrogen nuclei can actually be larger than the coupling between (like) ^{14}N nuclei. A detailed derivation for this case is given by Vega [40].

In many cases, the addition of a small magnetic field can change "semi-like nuclei" into "unlike nuclei," resulting in a significant increase in the spin-spin relaxation time.

## 2.3  INSTRUMENTATION

The basic physics for NQR signal detection is the same as for NMR signal detection. Hence, NQR spectrometers are similar to NMR spectrometers in design [41]. Of course NQR does not require a large external magnetic field and associated field control circuitry. High speed sample spinning, often used for NMR, is also not appropriate for NQR and will not be present. Since magnetic field homogeneity and spinning are not at issue, sample size is limited only by the available RF power and convenience.

Early NQR and NMR instruments were largely based on relatively simple oscillator designs including the super-regenerative oscillator [42], the

marginal oscillator [43], and the self-limiting "Robinson" oscillator circuit [44]. All of these are generally referred to as *continuous wave* (CW) techniques. For all of these oscillators the frequency is determined by an *LC* resonant circuit with the sample placed within (or near) the inductor *L*. The frequency is scanned by changing the capacitance *C*, either mechanically or electrically. Modern versions of these simple and inexpensive designs are still useful, particularly when searching for a signal over a broad range of frequencies and/or where small size is important [45]. Increasingly, however, computer-controlled pulsed spectrometers, similar to those now used for NMR, are employed for NQR. The sample is also within (or near) an inductor which is part of a tuned circuit, though the frequency is now determined by a separate reference oscillator.

For well-built NQR spectrometers, the principal source of electrical noise is the thermal noise from the *LC* tuned circuit. For best signal-to-noise ratios, care should be taken to minimize the resistive losses (i.e., maximize the quality factor) for that circuit. The signal-to-noise expected from an NQR measurement can be roughly estimated using expressions for an NMR measurement using the same nucleus at the same frequency [46–48].

In addition to the more common designs, several alternative techniques for NQR detection have been recently proposed, a few of which are also discussed below in Section 2.3.4.

## 2.3.1 CW Spectrometers

The use of a *marginal oscillator* for nuclear magnetic resonance originated with Pound and Knight [49, 50]. A number of transistorized versions of that circuit have appeared [51–54]. The marginal oscillator, as its name implies, uses just enough feedback to sustain low-level oscillations. That is, just enough energy is supplied by an active device (e.g., a transistor) as is lost and the behavior of the active device is still relatively linear. When additional energy is absorbed by the nuclei the level of oscillation can change significantly. The Robinson circuit, also now developed as a transistorized version for NQR [55], uses an additional bit of circuitry to maintain the level of feedback at a fixed value. The Robinson design is particularly useful for scans over a large frequency range.

The *super-regenerative spectrometer* is essentially a super-regenerative radio receiver but designed to detect the induced EMF from the nuclei rather than distant radio stations. An excellent explanation of how a super-regenerative receiver functions is presented by Insam [56]. In the super-regenerative circuit, the feedback condition is alternated between two states, one which maintains oscillations and one which does not. When switched from the non-oscillating or "quenched" state to the oscillating state, the time for the oscillations to build up to a predetermined level will depend on the

initial signal. That is, if one assumes an exponential growth in voltage starting at a value $V(0)$ and with a time constant $\tau$, the time $t$ to grow to a level $V_0 > V(0)$ is given by $t = \tau \ln\left(V_0 / V(0)\right)$.

Hence, in the presence of an induced EMF plus noise the oscillations will build up to the predetermined level sooner than with noise alone. The quenching signal may be generated by separate circuitry or one can design circuits which self quench. Due to the nonlinearity of the detection process (e.g., the logarithm above), one should not expect to obtain accurate line shapes with this type of spectrometer.

For the continuous wave (CW) techniques, and particularly for powder samples, additional sensitivity is often achieved using a set of external magnetic field coils which are switched on and off, combined with phase sensitive ("lock-in") detection. Typically 10–100 G fields are used at 10–100 Hz. When the magnetic field is on (with any polarity), the NQR signal is broadened sufficiently so that it is unobservable. Effectively, the magnetic field alternately turns the NQR signal on and off and only the change in the signal are recorded. Thus, all baseline errors are removed. Note that a similar technique is used for CW-NMR (usually with a sinusoidal magnetic field) resulting in a derivative signal. For NMR the magnetic field shifts the signal in frequency a bit rather than destroying it.

As an alternative to an on/off magnetic field, the frequency of an NQR oscillator circuit can be modulated electronically using a varicap diode or similar device as part of the $LC$ tuned circuit. With phase sensitive detection, one obtains a derivative signal (in the limit of small modulation) though often with significant baseline problems.

## 2.3.2 Pulsed Spectrometers

The electronics of pulsed NQR spectrometers is virtually identical to that of broad-band NMR spectrometers except without a large magnet. In fact, many pulsed NQR spectrometers are also used (with a magnet) as broad-band NMR spectrometers and vice versa. Since the pulsed method is much more versatile than the CW techniques, the vast majority of modern NQR measurements are made using pulse methods. Many of the pulse techniques began as NMR techniques and have been adapted to the NQR environment. Since significant inhomogeneous broadening is common in NQR (See section 2.2.5), one of the most important techniques is the use of spin-echoes, and related multiple-pulse techniques, for the study of these broadened lines.

A basic computer-controlled single channel pulsed NQR spectrometer is shown schematically in Figure 2.5. As is the case for NMR, the signals are often recorded in *quadrature*. That is, signals, which are in phase (cosine-like) and 90° out of phase (sine-like) with a stable reference source, are
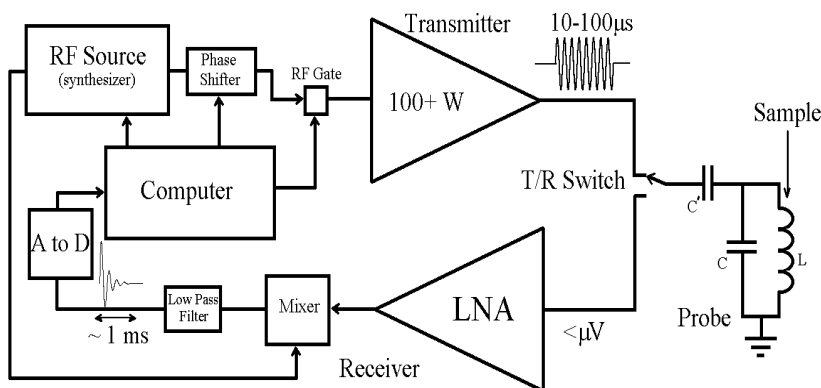
**Figure 2.5** Schematic of a simple computer-controlled pulsed NQR spectrometer.

simultaneously recorded in two channels. Due to their treatment under Fourier transform, and some carryover from CW-NMR terminology, these two signals are also sometimes referred to as the "real" and "imaginary" signals and/or "absorption" and "dispersion" signals, respectively. After heterodyning and filtering, the recorded signals have a frequency which is the difference between that of the RF reference and that of the nuclear magnetization. In many modern spectrometers, the analog to digital conversion is done before heterodyning, with the mixing and filtering performed digitally.

The transmit/receive (T/R) switch shown is usually implemented using passive circuitry. One common circuit is based on the scheme developed by Low and Tarr [57], which uses semiconductor diodes and quarter wavelength transmission lines. At frequencies below about 10 MHz, common in NQR, the quarter wavelength transmission lines are replaced with lumped circuit equivalents. Other tuned circuits using diodes can also be employed [58].

While the low noise amplifiers (LNAs) are protected from damage by such a passive T/R circuit, the receiver will be overdriven and there will be some "dead time" following the pulse while the receiving circuitry recovers. At lower frequencies this is exacerbated by the ringing of the *LC* tuned circuit containing the sample. When this ringing is a bad enough, additional circuitry can be added to damp the oscillations, such as a "Q-switch," and/or one can switch the phase of the applied RF pulse by 180° for a short time just before the RF is turned off. The latter approach can be quite demanding on the high power amplifier.

The simplest pulsed experiment is the application of a single pulse with a duration $\tau_p$ set to maximize the signal (1 to 100 μs typically). This is referred to as a 90° or $\pi/2$ pulse in analogy to the NMR case, though the simple classical picture, that this corresponds to a rotation of the nucleus by 90°, is

not valid. For powders, slightly longer pulses (approximately 30% longer) are used, compared to oriented single crystals, since many of the crystallites have a less than optimal orientation [59, 60]. The time-dependent signal after the pulse is referred to as the *free induction decay* (FID). If the spectral line shape is of interest, or in the rare case that there is more than one spectral line within the excitation band width (~10 kHz) then the signal will be Fourier transformed.

Simple spin-echoes are often very useful. The simplest is a two pulse measurement sometimes referred to as the *Hahn echo* with a 90° pulse, a time delay τ, a 180° pulse (twice the duration of a 90° pulse), followed by acquisition. The echo signal appears a time τ after the second pulse. All time-independent inhomogeneous interactions will be "refocused" by such a pulse sequence. Figure 2.6 illustrates FID (one pulse) and simple echo (two pulse) signals using one of the Br NQR transitions of $ZnBr_2$.
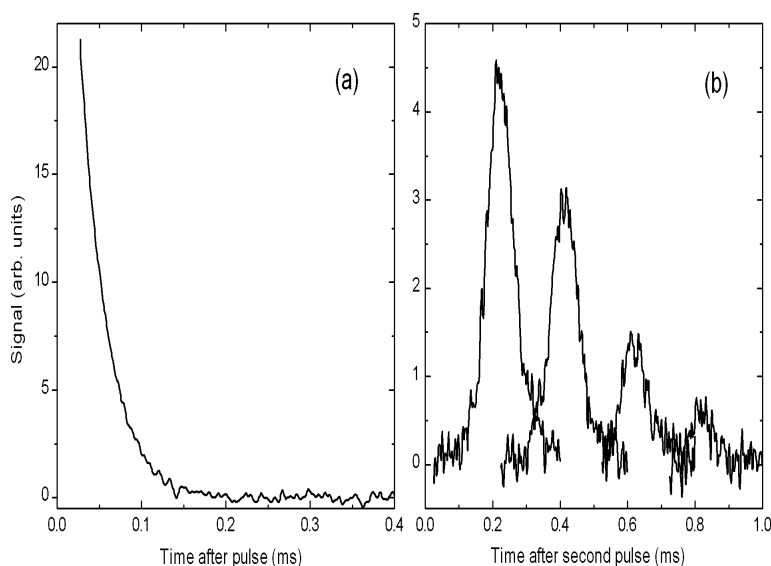


**Figure 2.6** Room temperature pulse NQR signals from the 79.75 MHz [81]Br transition in a powder sample of $ZnBr_2$ showing (a) a free induction decay (FID) after a single pulse and (b) echoes obtained using a two-pulse sequence for four different delay times (τ = 0.2, 0.4, 0.6, and 0.8 ms).

As is the case for NMR, phase shifts are often applied to the RF pulses and they are often labeled as they are in NMR. That is, a "$\pi/2_x$" pulse and a "$\pi/2_y$" pulse are 90° out of phase with each other. Phase cycling during signal averaging, in order to remove the effects of some spectrometer imperfections, is also common [61].

In the case of weaker signals, spin-echoes may be reformed many times using *steady state free precession* (SSFP) [62, 63] or *spin-lock spin-echo*
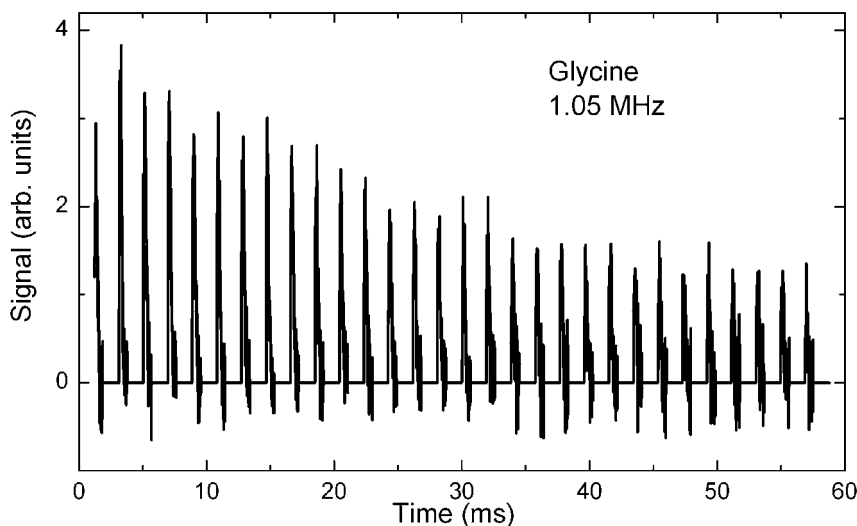
**Figure 2.7** Multiple $^{14}$N spin-echo signals from a spin-lock spin-echo (SLSE) pulse train. Data courtesy of J.B. Miller.

(SLSE) *pulse trains* [64, 65]. An example of such a measurement is shown in Figure 2.7.

Some more advanced work on pulse techniques includes the simultaneous excitation of two (or more) NQR transitions on the same nucleus [66–68] and various techniques to improve on the inherently inhomogeneous effective $B_1$ field for powder samples [69–71].

## 2.3.3 Field Cycling NQR Spectrometers

Field cycling spectrometers are often used to improve the sensitivity, particularly for low frequency NQR measurements and also in cases of low natural abundance. There are several different types of field cycling measurements referred to as NQR measurements – the most common are pulsed double resonance techniques where the actual measurement is an NMR measurement.

In a field cycling spectrometer the sample is alternatively subjected to a large magnetic field and a small (or zero) magnetic field. Since large magnetic fields are difficult to turn on and off rapidly, this is commonly achieved by physically moving the sample. Using pneumatics, this can be routinely accomplished over a distance of about 1 m in about 100 ms or less.

In its simplest form, the sample is placed in a very high magnetic field to obtain a large nuclear splitting and hence a large population difference. After

equilibrium is reached, the magnetic field is reduced and RF is applied at the NQR frequency, the magnetic field is reintroduced, and an NMR measurement is performed. This method can be applied to half-integer spins directly [72] or for any spin using double resonance [73]. For the latter, $^1$H is most often used as the second nucleus since it is easily observed using NMR.

For double resonance one relies on "contact" between the two nuclei some time during the measurement. Contact here refers to the case where the nuclear energy level splittings for the two nuclei match and the nuclei are physically close enough so that they can interact (e.g., via the nuclear magnetic dipole interaction). That match can occur either in the presence or absence of RF irradiation(s). When there is a match, there is efficient transfer of energy between the two types of nuclei in the same way there is transfer of energy between two weakly coupled, identical pendulums.

In an alternative form useful for compounds that contain hydrogen, the large polarizations that can be achieved for $^1$H in a high magnetic field can be transferred, in part, to the nucleus to be measured and then a traditional NQR measurement is made. While not as sensitive, this technique has the advantage that a highly uniform magnetic field is not required for the NMR measurement. For example, initial exposure to the nonuniform magnetic field of permanent magnets can be used to obtain a large, though non-uniform, initial $^1$H polarization, which can then be transferred to $^{14}$N prior to an NQR measurement [74].

## 2.3.4 Some Less Common NQR Detection Schemes

The direct NQR techniques mentioned above all rely on Faraday's law of induction. Since the signal is generated by the time rate of change of the magnetic flux, these techniques lose sensitivity at low frequencies. In contrast, in a growing number of cases it is possible to detect the magnetic flux directly, rather than its time derivative. At present, these alternative detection schemes are difficult to implement on a routine basis.

A *superconducting quantum interference device*, or SQUID, is sensitive to magnetic flux and can have a very low noise level. For use as a pure NQR detector, the time-dependent nuclear magnetization is detected after a perturbation. Unlike the NMR case, however, there is no static nuclear magnetization. NQR signals have been detected using a SQUID at frequencies as low as few tens of kHz up to about 1 MHz [75–78].

A second flux detection technique recently proposed for NQR utilizes an optical transition in an alkali metal vapor in a way that is very sensitive to magnetic fields [79]. It is, in essence, a form of optically detected electron paramagnetic resonance (EPR) in a very weak static magnetic field. For NQR detection the time-dependent resonant magnetic field is supplied by the precession of the nearby nuclear magnetic moments to be detected.

A disadvantage for many pulsed NQR measurements at lower frequencies is the "dead time" after an applied pulse. Eles and Michal [80] have recently developed a method for spin 3/2 using a strong excitation at half the resonant frequency yielding a two-photon excitation, followed by traditional detection. The advantage is that the excitation frequency is well-separated from the receiver frequency, thus allowing the dead time to be virtually eliminated.

Another interesting NQR technique, which does not rely on magnetic flux at all was recently reported [81]. A close relative of *perturbed angular correlation* (PAC) techniques, the β-decay is measured from radioactive $^8$Li nuclei after they are implanted in a material using a polarized beam. The β particles are then emitted in a direction determined by the nuclear polarization. A resonant sinusoidal magnetic field alters the nuclear polarization and thus affects the β count rate. While the number of isotopes available for such studies may be limited, it is noted that only about $10^7$ nuclei are required for this technique, far fewer than are required for other NQR techniques.

## 2.4  INTERPRETATION OF COUPLING CONSTANTS

The contribution of the electric quadrupole field (*eq* in $e^2qQ$) can be computed for a known charge distribution surrounding a nucleus. From that the coupling constant can be estimated and compared to experiment. With modern computational techniques for materials, the largest uncertainty is often that due to the uncertainty in nuclear electric quadrupole moment, $Q$. For many measurements, however, of most importance are the relative changes from one situation to another, and not the absolute values. For example, one might be concerned with the differences in bonding between two similar compounds, one may be studying structural changes in the lattice during a phase transition, or one might be concerned with general correlations between NQR and other properties [82].

There are three broad situations encountered for electric quadrupole field calculations. The easiest to handle are molecular crystals where the charge distribution near the nucleus is predominantly determined by covalent bonds. For those compounds, relatively straightforward molecular computations can be made and one can expect only a small "solid effect" due to the stacking of molecules within the crystal structure. The two other cases are for ionic and metallic materials, respectively.

The electric quadrupole field at the origin due to a point charge of magnitude 1 (in cgs units) at a position $(x_1, x_2, x_3) = (x, y, z)$ relative to a nucleus at the origin is found by taking the second derivatives of the usual Coulomb potential. That computation gives

$$V_{ij} = \frac{1}{r^3}\left(\frac{3x_i x_j}{r^2} - \delta_{ij}\right),$$

where $r$ is the distance to the origin. Since superposition applies, the field from a charge distribution is computed as the sum of the contributions from all the charges involved. Due to the $1/r^3$ dependence and charge neutrality within a unit cell, the most important contributions are those due to charges near the nucleus.

## 2.4.1 Molecular Crystals and Covalently Bonded Groups

Electron wavefunctions, and hence quadrupole coupling constants, can be easily computed using *ab initio* computation techniques. To understand and describe trends, however, it is often convenient to describe the electron wavefunctions in covalently bonded systems using a *linear combination of atomic orbitals* (LCAO) approach. Since filled electron (atomic) shells have a spherical charge distribution, only the outer electrons need be considered. There is also a response of the inner core electrons to the presence of an electric field gradient, which is quite important but which is ignored for the moment.

Consider an occupied electronic $p_z$-orbit which is (quite generally) described by a wavefunction $\psi$, as

$$\psi = \left( \frac{1}{2} \sqrt{\frac{3}{\pi}} \, \cos\theta \right) f(r) \qquad (2.40)$$

where $f(r)$ is the (separately normalized) radial part of the wavefunction and, of course, $\cos\theta = z/r$. Then, for example,

$$V_{zz} = -e \int\limits_{r=0}^{\infty} \int\limits_{\varphi=0}^{2\pi} \int\limits_{\theta=0}^{\pi} \psi^* \, \frac{3\cos^2\theta - 1}{r^3} \, \psi \, r^2 \sin\theta \, d\theta \, d\varphi \, dr$$

$$= -\frac{3e}{2} \int\limits_{r=0}^{\infty} \frac{1}{r^3} \, r^2 |f(r)|^2 \int\limits_{\theta=0}^{\pi} \cos^2\theta \left( 3\cos^2\theta - 1 \right) \sin\theta \, d\theta \, dr$$

$$= -\frac{4e}{5} \int\limits_{r=0}^{\infty} \frac{1}{r^3} r^2 |f(r)|^2 \, dr = -\frac{4e}{5} \left\langle \frac{1}{r^3} \right\rangle \equiv e \, q_p \qquad (2.41)$$

and similarly for other terms and other orbitals. Note that $\left\langle 1/r^3 \right\rangle \approx 1/a_0^3$, where $a_0$ is the Bohr radius, so $V_{zz} \approx 10^{18}$ V/cm/cm . Values of $\left\langle 1/r^3 \right\rangle$ from nonrelativistic [83] and relativistic [84] atomic calculations are available.

For a more general combination of atomic orbitals the following should be noted [85, 86]. First, s-orbitals are spherical and do not contribute. Furthermore, cross-terms involving s-orbitals and p-orbits, and p-orbitals and d-orbitals are zero due to symmetry within the integral. Cross-terms between s- and d-orbitals are usually neglected. For molecular wavefunctions using the

LCAO-MO picture, the contributions from orbitals on other atoms will be small.

Hence, with $a_x^2$, $a_y^2$, and $a_z^2$ the respective weights for $p_x$, $p_y$, and $p_z$ contributions to the wavefunction from orbitals on the atom in question, one gets

$$V_{zz} = e\,q_p \left[ 3a_z^2 - \left(a_x^2 + a_y^2 + a_z^2\right) \right] / 2$$
$$V_{xx} = e\,q_p \left[ 3a_x^2 - \left(a_x^2 + a_y^2 + a_z^2\right) \right] / 2 \qquad (2.42)$$
$$V_{yy} = e\,q_p \left[ 3a_y^2 - \left(a_x^2 + a_y^2 + a_z^2\right) \right] / 2$$

and note that $a_x^2 + a_y^2 + a_z^2 \leq 1$ though the entire wavefunction must be normalized. If there is a small s or d contribution to the wavefunction, the largest impact on the electric field gradient is likely via the reduction in the weights for the p-orbitals. The total electric field gradient is computed using the sum of the contributions from all the occupied valence wavefunctions.

## 2.4.2 Ionic Crystals

In principle, the computation of the electric field gradient in an ionic material is straightforward. The ions are replaced by point charges and the appropriate lattice sums are performed [87]. To achieve accurate values and reasonably fast convergence, it is necessary to take some care in the way the sum is computed.

To understand why care must be exercised, consider the following inaccurate method. First the contribution from all the negative charges is added out to a large distance $R$. Then, the contributions from the positive charges are added, again out to the distance $R$. The two sums are then subtracted from one another. Such a technique fails since the quadrupole field falls as $1/r^3$ but the number of neighboring ions in a spherical shell a distance $r$ away grows as $r^2$. Hence, the total contribution falls as $1/r$, and the individual sums tend to diverge. The net result is the relatively small difference between two very large values. Furthermore, the use of an arbitrary cut-off $R$ does not guarantee that the total calculation is charge neutral, which can lead to a significant systematic error.

To obtain accurate values and rapid convergence, terms in these lattice sums should be grouped appropriately. A simple method which has rapid convergence is to use a sum over conventional unit cells where the nucleus in question has been centered. In addition, ions of charge $q$ which are on the boundary of $n$ conventional unit cells are included in all of the unit cells, but with a charge $q/n$ for each [88]. The use of a conventional unit cell ensures that charge neutrality and the symmetry of the crystal are included at every step. The field produced from each neighboring unit cell will be that of an electric dipole, or more often a higher order multipole, which will fall off much faster with distance than that of a point charge.

For numerical computations terms of comparable magnitude should be grouped together. Symbolically, the appropriate lattice sum would then be

$$
V_{ij} = \sum_{\substack{\text{all } R}} \left\{ \sum_{\substack{\text{unit cells at} \\ \text{distance R}}} \left[ \sum_{\substack{\text{ions in conven-} \\ \text{tional unit cell}}} \frac{q}{r^3} \left( \frac{3x_i x_j}{r^2} - \delta_{ij} \right) \right] \right\} \tag{2.43}
$$

where $r$ is the total distance from the origin to the ion and $q$ is the appropriate, possibly fractional, charge for that ion. Alternative approaches include the explicit use of multipole expansions and/or the Fourier transformation of the lattice.

Field gradients computed using this type of point charge model for the ions will certainly need to be corrected as discussed below in Section 2.4.4.

## 2.4.3 Metals

A very simple model for a metal is the "uniform background lattice," where the conduction electrons are considered to be uniformly distributed and the remaining positive ions are treated as point charges [89]. To achieve convergence for the electric quadrupole field, charges near the origin need to be avoided, however. Metals with narrow conduction bands can often be treated using the tight binding model, which is treated as in Section 2.4.1. To go much beyond these simple models the problem becomes very complicated very quickly and will depend on the specific metal being considered. The interested reader is referred to the review articles by Kaufmann and Vianden [90] and by Das and Schmidt [91].

For simple metals the temperature dependence of the quadrupole coupling often varies as the 3/2 power of the (absolute) temperature. That is

$$
\nu_Q(T) = \nu_Q(0) \left( 1 - \alpha T^{3/2} \right), \tag{2.44}
$$

where $\alpha$ is a constant. This temperature dependence is associated with the changes in the electronic structure in the presence of thermal vibrations [92].

## 2.4.4 Sternheimer Shielding/Antishielding

The slight rearrangement of the core electrons in the presence of an electric field gradient has so far been neglected. A series of works by Sternheimer [93] has shown, however, that the effects on the observed quadrupole coupling constant can be far from negligible. There are two Sternheimer shielding factors which are usually considered, one associated with charges which are on the atom (or ion) in question, $R$, and one associated with more distant charges, $\gamma_\infty$. These factors are often negative and are then referred to as "antishielding" factors. If $eq_{\text{atomic}}$ is the magnitude of the computed electric

field gradient associated with electrons on the atom (e.g., the valence electrons) and $eq_{ext}$ is that due to charges on other atoms, then the observed value $eq_{obs}$ is predicted to be

$$eq_{obs} = eq_{atomic} \ \ (1 - R) \ + \ eq_{ext}(1 - \gamma_\infty) \ . \tag{2.45}$$

More rigorously the atomic and external terms should be combined as tensor, rather than scalar, quantities. Table 2.3 shows a selection of typical shielding values for $\gamma_\infty$.

**Table 2.3** Typical Sternheimer factors for several ions.

| Atom/Ion | $\gamma_\infty$ |
|----------|-----------------|
| Na | −3.7 |
| $Na^+$ | −3.7 |
| $Al^{2+}$ | −1.8 |
| $Cl^-$ | −60 |
| $Br^-$ | −110 |
| $Rb^+$ | −50 |
| $I^-$ | −160 |

Agreement between $\gamma_\infty$ values computed using different methods is no better than ±10% and in many cases much worse. It is clear, however, that the correction can be quite large. Computed values for $R$ can be so dependent on the specific electronic configuration used that one is prone to wonder about the utility of having such values. In the majority of cases, $R$ is of order 0.1.

Of course, a rigorous *ab initio* computation of the electronic structure of a material (including the core electrons, band structure effects, etc.) will not require these additional corrections. Computer codes available for electronic structure calculations are often optimized for computations of energies, rather than electron densities, and hence any quadrupole coupling constants produced from such programs should be used with caution.

## 2.5 SUMMARY

NQR is a radio frequency spectroscopy akin to wide line NMR but without a large magnet. NQR uses nuclei with spin I > ½ to probe the environment in a material. The NQR frequency will be determined by the (time-averaged) distribution of electric charge in the vicinity of a nucleus, and that distribution depends on the material being investigated. The quadrupole coupling constant, the relaxation times after an excitation, and the effects of small magnetic fields, along with modeling and comparison to other similar materials, are used to extract information about the material.

# Bibliography

For additional general information, interested readers should consult one or more of the following:

Nuclear quadrupole resonance spectroscopy, T.P. Das and E.L. Hahn, Supplement 1 of *Solid State Physics* (Academic Press, NY, 1958).

Nuclear quadrupole resonance spectroscopy, E. Schempp and P.J. Bray, Chapter 11 of *Physical Chemistry, An Advanced Treatise, Vol IV, Molecular Properties*, D. Henderson (ed.), pages 521–632 (Academic Press 1970).

Nuclear quadrupole resonance spectroscopy, J.A.S. Smith, *J. Chem. Education*, Vol 48, Nos. 1–4, pages 39–49, A77–A89, A147–A148, A159–170, and A243–A252, (1971).

Nuclear quadrupole resonance in inorganic chemistry, Yu. A. Buslaev, E.A. Kravcenko, and L. Kolditz, published as Volume 82 or Coordination Chemistry Reviews (Elsevier, Amsterdam, 1987).

*Nuclear Quadrupole Coupling Constants*, Lucken E.A.C (Academic Press, London and New York, 1969).

*Principles of Nuclear Magnetism*, A. Abragam (Oxford Univ. Press, Oxford, 1961).

*Principles of Magnetic Resonance*, 3$^{rd}$ Ed., C.P. Slichter, (Springer-Verlag, Heidelberg, 1989).

*Experimental Pulse NMR – A Nuts and Bolts Approach*, E. Fukushima and S.B.W. Roeder (Addison-Wesley Publishing, Reading, MA, 1981).

# REFERENCES

[1]  Pound, R.V. (1950) *Phys. Rev.* **79**, 685-702.

[2]  Dehmelt, H.G. & Kruger, H. (1950) *Naturwiss*. **37**, 111-112.

[3]  Das, T.P. & Hahn, E.L. (1958) *Nuclear Quadrupole Resonance Spectroscopy, Supplement 1 of Solid State Physics,* Seitz F. & Turnbull D. (eds) (New York, Academic).

[4]  Ohte, A., Iwaoka, H., Mitsui, K., Sakurai, H. & Inaba, A. (1979) *Metrologia* **15**, 195-199.

[5]  Huebner, M., Leib, J. & Eska, G. (1999) *J. Low Temp. Phys.* **114**, 203-230.

[6]  Garroway, A.N., Buess, M.L., Miller, J.B., Suits, B.H., Hibbs, A.D., Barrall, G.A., Matthews, R. & Burnett, L.J. (2001) *IEEE Trans. Geosci. Remote Sens.* **39**, 1108-1118.

[7]  Segel, S.L. (1978) *J. Chem. Phys*. **69**, 2434-2438.

[8]  Thyssen, J., Schwerdtfeger, P., Bender, M., Nazarewicz, W. & Semmes, P.B. (2001) *Phys. Rev. A* **63**, 022505:1-11.

[9]  Gerginov, V., Derevianko, A. & Tanner, C.E. (2003) *Phys. Rev. Lett*. **91**, 072501:1-4.

[10]  Slichter, C.P.  (1990) *Principles of Magnetic Resonance, 3$^{rd}$ Ed.,* (Heidelberg, Springer-Verlag)

[11]  Bain, A.D. & Khasawneh, M. (2004) *Concepts Magn. Reson.* **22A**, 69-78.

[12]  Butler, L.G. & Brown, T.L. (1981) *J. Magn. Reson.* **42**, 120-131.

[13]  Hiyama, Y., Butler, L.G. & Brown, T.L. (1985) *J. Magn. Reson.* **65**, 472-480

[14]  Cohen, M.H. (1954) *Phys. Rev*. **96**, 1278-1284.

[15]  Bersohn, R. (1952) *J. Chem. Phys*. **20**, 1505-1509.

[16]  Wang, T-C. (1955) *Phys. Rev*. **99**, 566-577.

[17]  Suits, B.H. & Slichter, C.P. (1984) *Phys. Rev.* B **29**, 41-51.

[18]  Sundfors, R.K., Bolef, D.I. & Fedders, P.A. (1983) *Hyperfine Interactions* **14**, 271-313.

[19]  Lee, Y.K. (2002) *Concepts Mag. Reson*. **14**, 155-171.

[20]  Vega, S. (1978) *J. Chem. Phys.* **68**, 5518-5527.

[21]  Sauer, K.L., Suits, B.H., Garroway, A.N. & Miller, J.B. (2001) *Chem. Phys. Lett.* **342**, 362-368; (2003) *J. Chem. Phys*. **118**, 5071-5081.

[22]  Raich, J.C. & Good Jr. R.H. (1963) Am. *J. Physics* **31**, 356-362.

[23]  Bloom, M., Hahn, E.L. & Herzog B. (1955) *Phys. Rev.* **97**, 1699-1709.

[24]  Muha, G.M. (1980) *J Chem Phys* **73**, 4139-4140; (1982) *J. Magn. Reson.* **49** 431-443.

[25]  Brooker, H.R. & Creel, R.B. (1974) *J. Chem. Phys.* **61**, 3658-3664.

[26]  Bloom, M. (1954) *Phys. Rev.* **94,** 1396-1397.

[27]  Creel, R.B., von Meerwall, E.D. & Brooker, H.R. (1975) *J. Magn. Reson.* **20**, 328-333.

[28]  Sunitha, Bai N., Reddy, N. & Ramachandran, R. (1993) *J. Magn. Reson*. *A* **102**, 137-143.

[29]  Chen, M.C. & Slichter, C.P. (1983) *Phys. Rev. B* **27**, 278-292.

[30]  Korringa, J. (1950) *Physica* **16**, 601-610.

[31]  For Example see Martindale, J.A., Barrett, S.E., Durand, D.J., O'Hara, K.E., Slichter, C.P., Lee, W.C. & Ginsberg, D.M. (1994) *Phys. Rev.* B **50**, 13645-13652.

[32]  Matsamura, M., Saskawa, T., Takabatake, T., Tsuji, S., Tou, H. & Sera, M. (2003) *J. Phys. Soc. Japan* **72**, 1030-1033.

[33]  Bayer, H. (1951) *Z. Physik* **130**, 227-238.

[34]  Kushida, T., Benedek, G.B. & Bloembergen, N. (1956) *Phys. Rev*. **104**, 1364-1377.

[35]  Schempp, E. & Silva, P.R.P. (1973) *Phys. Rev. B* **7** 2983-2986; (1973) *J. Chem. Phys.* **58**, 5116-5119.

[36]  Alexander, S. & Tzalmona, A. (1965) *Phys. Rev.* **138**, A845-A855.

[37]  van Vleck, J.H. (1948) *Phys. Rev.* **74**, 1168-1183.

[38]  Abgragam, A. & Kambe, K. (1953) *Phys. Rev.* **91**, 894-897.

[39]  Nagel, O.A., Ramia, M.E. & Martin, C.A. (1996) *Appl. Magn. Reson.* **11**, 557-566.

[40]  Vega, S. (1973) *Advances in Magn. Reson.* **6**, 259-302.

[41]  Suits, B.H. (1994) in Trigg G. L. (ed.) *Encyclopedia of Applied Physics, Vol. 9*, 71-93 (VCH Publishers).

[42]  Roberts, A. (1947) *Rev. Sci. Instrum.* **18**, 845-848.

[43]  Pound, R.V. & Knight, W.D. (1950) *Rev. Sci. Instrum.* **21**, 219-225.

[44]  Robinson, F.N.H. (1959) *J. Sci. Instrum*. **36,** 481-487.

[45]  Kim, S.S., Mysoor, N.R., Carnes, S.R., Ulmer, C.T. & Halbach, K. (1997) In *Proceedings of the 16th Digital Avionics Systems Conference (DASC)*, Irvine, CA, (IEEE, New Jersey), pp. 2.2-14-2.2-23.

[46]  Hill, H.D.W. & Richards, R.E. (1968) *J. Phys. E: Sci. Inst. Series* 2, **1**, 977-983.

[47]  Hoult, D.I. & Richards, R.E. (1976) *J. Magn. Reson*. **24**, 71-85.

[48]  Hoult, D.I. (1973) *Prog. NMR Spec*. **12**, 41-77.

[49]  Pound, R.V. & Knight, W.D. (1950) *Rev. Sci. Instrum*. **21**, 219-225.

[50]  Pound, R.V. (1952) *Prog. Nucl. Phys*. **2**, 21-50.

[51]  Viswanathan, T.L., Viswanathan, T.R. & Sane, K.V. (1968) *Rev. Sci. Instrum*. **39**, 472-475; (1970) *Rev. Sci. Instrum.* **41**, 477-478

[52]  Zikumaru, Y. (1990) *Z. Naturforsch.* **45a**, 591-594.

[53]  Sullivan, N. (1971) *Rev. Sci. Instrum.* **42**, 462-465.

[54]  Offen, R.J. & Thomson, N.R. (1969) *Phys. Educ*. **4**, 264-267.

[55]  Robinson, FNH. (1982) *J. Phys. E: Sci. Instrum*. **15**, 814-823.

[56]  Insam, E. (2002) *Electronics World* **108**(1792) 46-53.

[57]  Lowe, I.J. & Tarr, C.E. (1968) *J. Phys. E: Sci. Instrum.* **1**, 320-322.

[58]  McLachlan, L.A. (1980) *J. Magn. Reson.* **39**, 11-15.

[59]  Bloom, M., Hahn, E.L. & Herzog, B. (1955) *Phys. Rev.* **97**, 1699-1709.

[60]  Vega, S. (1974) *J. Chem. Phys.* **61**, 1093-1100.

[61]  Stejskal, E.O. & Schaefer, J. (1974) *J. Magn. Reson*. **13**, 249-251.
[62]  Bradford, R., Clay, C. & Strick, E. (1951) *Phys. Rev.* **84**, 157-158.
[63]  Rudakov, T.N., Mikhaltsevitch, V.T., Flexman, J.H., Hayes, P.A., & Chisholm, W.P. (2004) *Appl. Magn. Reson.* **25**, 467-474.
[64]  Marino, R.A. & Klainer, S.M. (1977) *J. Chem. Phys.* **67**, 3388-3389.
[65]  Cantor, R.S. & Waugh, J.S. (1980) *J. Chem. Phys.* **73**, 1054-1063.
[66]  Grechishkin, V.S., Anferov, V.P. & Ja., N. (1983) *Adv. Nucl. Quadrupole Reson.***5** 1; Greschishkin, V.S. (1990) *Z. Naturforsch.* **45a**, 559-564.
[67]  Sauer, K.L., Suits, B.H., Garroway, A.N. & Miller, J.B. (2001) *Chem. Phys. Lett*. **342**, 362–368; (2003) *J. Chem. Phys*. **118**, 5071-5081.
[68]  Furman, G.B. & Goren, S.D. (2002) *Z. Naturforsch.* **57a** 315-319.
[69]  Miller, J.B., Suits, B.H., Garroway, A.N. (2001) *J. Magn. Reson.* **151,** 228-234.
[70]  Miller, J.B. & Garroway, A.N. *Appl. Magn. Reson.* **25**, 475-483.
[71]  Ramamoorthy, A. & Narasimhan, P.T. (1990) *Z. Naturforsch* **45a** 581-586.
[72]  Ivanov, D. & Redfield, A.G. (2004) *J. Magn. Reson*. **166**, 19-27.
[73]  Slusher, R.E. & Hahn, E.L. (1968) *Phys. Rev.* **166**, 332-347.
[74]  Luznik, J., Pirnat, J. & Trontelj, Z. (2002) *Sol. State Commun.* **121**, 653-656.
[75]  Hürlimann, M.D., Pennington, C.H., Fan, N.Q., Clarke, J., Pines, A. & Hahn, E.L. (1992) *Phys. Rev. Lett*. **69**, 684-687.
[76]  TohThat, D.M. & Clarke, J. (1996) *Rev. Sci. Instrum.* **67**, 2890-2893.
[77]  Augustine, M.P., TohThat, D.M. & Clarke, J. (1998) *Solid State Nucl. Magn. Reson*. **11**, 139-156.
[78]  Greenberg, Ya.S. (1998) *Rev. Mod. Phys*. **70**, 175-222; 2000 *Rev. Mod. Phys.* **72,** 329.
[79]  Savukov, I.M., Seltzer, S.J., Romalis, R.V. & Sauer, K.L. (2005) *Phys. Rev. Lett*. **95**, 063004:1-4.
[80]  Eles, P.T. & Michal, C.A. (2005) *J. Magn. Reson.* **175**, 201-209.
[81]  Salman, Z., Reynard, E.P., MacFarlane, W.A., Chow K. H., Chakhalian, J., Kreitzman, S.R., Daviel, S., Levy, C.D.P., Poutissou, R. & Kiefl, R.F. (2004) *Phys. Rev. B* **70**, 104404:1-7.
[82]  Weiss, A. & Wigand, S. (1990) *Z. Naturforsch* **45a**, 195-212.
[83]  Fischer, C.F. (1977) *The Hartree-Fock Method for Atoms* (Wiley & Sons, NY).
[84]  Lindgren, I. & Rosén, A. (1974) *Case Studies Atomic Phys*. **4**, 197-298.
[85]  Townes, C.H. & Dailey, B.P. (1949) *J. Chem. Phys.* **17**, 782-796.
[86]  Schempp, E. & Bray, P.J. (1970) Vol. IV, Chap. 11 of Henderson D (ed.) *Physical Chemistry: An Advanced Treatise*, Academic Press, New York, London.
[87]  Hutchings, M.T. in Seitz, F. & Turnbull, D. (eds.) (1964) *Solid State Physics* **16** *(Academic Press, New York and London),* 227-273.
[88]  Frank, F.C. (1950) *Philos. Mag.* **41**, 1287-1289.
[89]  de Wette, F.W. & Schacher, G.E. (1965) *Phys. Rev*. **137**, A92-A94.
[90]  Kaufmann, E.N. & Vianden, R.J. (1979) *Rev. Mod. Phys*. **51**, 161-214.
[91]  Das, T.P. & Schmidt, P.C. (1986) *Z. Naturforsch* **41a**  47-77.
[92]  Jena, P. (1976) *Phys. Rev. Lett*. **36**, 418-421.
[93]  Sternheimer, R.M. (1951) *Phys. Rev.* **84**, 244-253; 1951 *Phys. Rev*. **86**, 316-324; 1954 *Phys. Rev*. **95**, 736-750; 1986 *Z. Naturforsch* **41a**, 24-36.